

## **THE INFLUENCE OF SURFACE ROUGHNESS ON THE FATIGUE PERFORMANCE OF SELECTIVE LASER MELTED ALUMINIUM ALLOY A357**

\*Jeremy H. Rao<sup>1,2</sup>, Kai Zhang<sup>1,3</sup>, Paul Rometsch<sup>1,2</sup>, Aijun Huang<sup>1,2</sup>, and Xinhua Wu<sup>1,2</sup>

<sup>1</sup> *Monash Centre for Additive Manufacturing, 15-17 Normanby Road, Notting Hill, VIC 3168, Australia*

<sup>2</sup> *Department of Materials Science and Engineering, Monash University, Clayton, VIC 3800, Australia*

<sup>3</sup> *Department of Mechanical and Aerospace Engineering, Monash University, Clayton, VIC 3800, Australia*  
(\*Corresponding author: [Jeremy.rao@monash.edu](mailto:Jeremy.rao@monash.edu))

### **ABSTRACT**

As one of the most typical additive manufacturing (AM) technologies, selective laser melting (SLM) removes many of the shape restrictions that limit materials design, thereby allowing computationally optimised and high performance structures to be directly produced and tested. Due to the high reflectivity and lower absorptivity of Al alloy A357 powder during high temperature laser melting, one of the issues SLM might bring is the surface roughness and defects present on the parts. In this regard, this study investigates the surface roughness – fatigue property relationship for a heat-treated aluminium alloy A357 after SLM. Via the adjustment of SLM parameters, an ultrafine microstructure can be obtained due to the fast solidification rate. Therefore, comparable or even better mechanical properties can be achieved with respect to traditional A357 casting counterparts. Meanwhile, the surface roughness conditions of the SLMed Al alloy are also influenced by various processing parameters, raw powder properties, and sample building methods. For selective laser melted Al alloy A357 specimens, a dense part with a smoother surface would be expected to correspond with a good fatigue performance.

### **KEYWORDS**

Al-Si alloys, Microstructure, Heat treatment, Fatigue properties, Selective laser melting

## INTRODUCTION

Additive Manufacturing (AM), also known as 3D printing, is a process in which a complex part is fabricated layer by layer from a digital design package (Martin et al., 2017). AM has the potential to conserve raw materials, reduce the energy consumption, part cost, and fabrication time. Furthermore, as a typical additive manufacturing (AM) process, selective laser melting (SLM) was originally developed from selective laser sintering (SLS) based on higher quality lasers (Rao, Zhang, Fang, Chen, Wu, & Davies, 2017b). Different from conventional casting consuming valuable time and energy, SLM is now used as a cost effective method for the manufacturing of metals, such as Al-Si alloys, to produce almost full density parts using fine metallic powder and high power laser beam (Tang & Pistorius, 2017).

Cast aluminium alloys have been attractive alternatives to some conventional steels due to their higher corrosion resistance. Also, Al alloys are mainly used for the production of parts requiring high thermal conductivity and reasonably good mechanical properties at different heat treatment conditions (Prashanth, Scudino, & Eckert, 2017; Rao, Wu, & Davies, 2017a). The material costs are also much lower compared to titanium and nickel alloys in a SLM manufacturing field (Rao, Giet, Yang, Wu, & Davies, 2016). As a typical cast alloy, aluminium alloy A357 is suitable for light weight construction and at the same time meet the requirements of structural durability, and thus are highly demanded in a variety of engineering fields (Rao et al., 2017b).

In order to extend the applications of SLM process in aerospace and automotive industries, the selective laser melted parts are also required to be durable under both static and cyclic loading (Brandl, Heckenberger, Holzinger, & Buchbinder, 2012; Siddique, Imran, & Walther, 2017). Therefore, there is a need for in-depth investigation on a variety of mechanical properties especially fatigue performance, since it is closely related to the presence of defects and surface roughness of selective laser melted aluminium alloys (Aboulkhair, Maskery, Tuck, Ashcroft, & Everitt, 2016; Uzan, Shneck, Yeheskel, & Frage, 2017). Although a series of authentic work about the influence of microstructure and defects on the fatigue resistance of different SLMed Al alloys has been investigated (Aboulkhair et al., 2016; Brandl et al., 2012; Siddique et al., 2017; Tang & Pistorius, 2017; Uzan et al., 2017), quite few of them have applied the SLM technique to Al alloy A357, and the correlation of the fatigue performance to the surface roughness features has been less frequently studied as well. In this regard, this paper will focus on the effects of processing parameters on the morphology of SLMed sample surface, which would eventually influence the mechanical properties of SLMed Al alloy A357 parts to various scales.

## EXPERIMENTAL

The particle size distribution of the Al alloy A357 powder was measured and analysed by “Malvern Mastersizer 2000” machine. The raw powder possesses a spherical shape (Figure 1a) with the volume weighted mean diameter of approximately 40  $\mu\text{m}$  (Figure 1b). The material used in this study was gas atomised Al alloy A357 powder supplied by TLS Technik, with the main chemical compositions determined in Table 1.

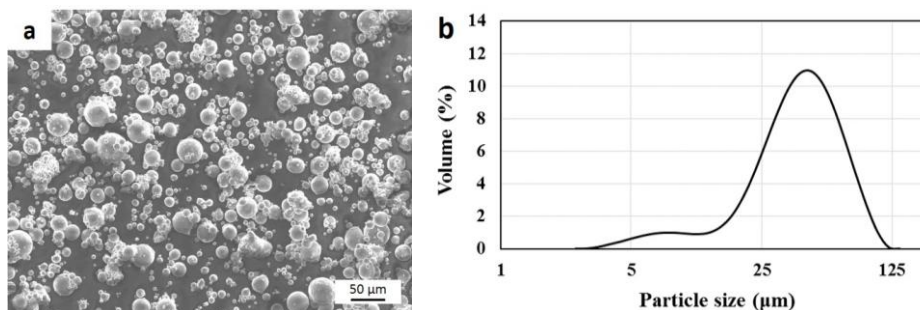


Figure 1. (a) SEM micrograph showing the particle size and the morphology of Al alloy A357 powder; (b) the volume weight percent powder size distribution

Table 1. Chemical compositions of the Al alloy A357 determined by ICP-AES (wt. %)

| Alloy element | Al  | Si   | Mg   | Fe   | Ti   | Ni   | Mn   | Cu    | Zn    |
|---------------|-----|------|------|------|------|------|------|-------|-------|
| A357          | Bal | 7.01 | 0.62 | 0.15 | 0.02 | 0.01 | 0.01 | <0.01 | <0.01 |

The particular SLM process in this work was conducted by an X LINE 1000R powder-bed machine, with an alternating scan strategy used to build each part (Figure 2).

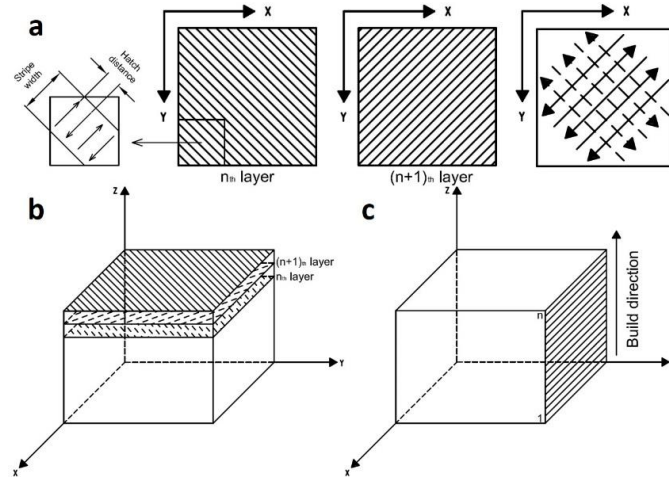


Figure 2. (a) The scanning strategy used to build SLMed samples; the deposit layers in SLM from (b) the top view (xy-plane), and (c) the side view (z-plane)

Two groups of fatigue samples, group A and B, were built normal to the build direction (BD) z in order to optimise the surface roughness of the SLMed parts. Each group contained 9 samples (plus a spare one), which differed from others by a wide range of parameters, such as laser powers ranging from 200 to 750 W, scan speeds from 600 to 2000 mm/s, hatch distances from 0.1 to 0.3 mm, powder layer thicknesses from 40 to 60  $\mu\text{m}$ , and contour offsets from 0.02 to 0.4 mm (Fox, Moylan, & Lane, 2016; Wang, Sin, Nai, & Wei, 2017). We defined these two groups of samples based on their geometries (Figure 3):

- A. Net-shaped low cycle fatigue samples: directly built into the final geometry as designed;
- B. Cylindrical low cycle fatigue samples: built into a cylindrical shape for post-machining.

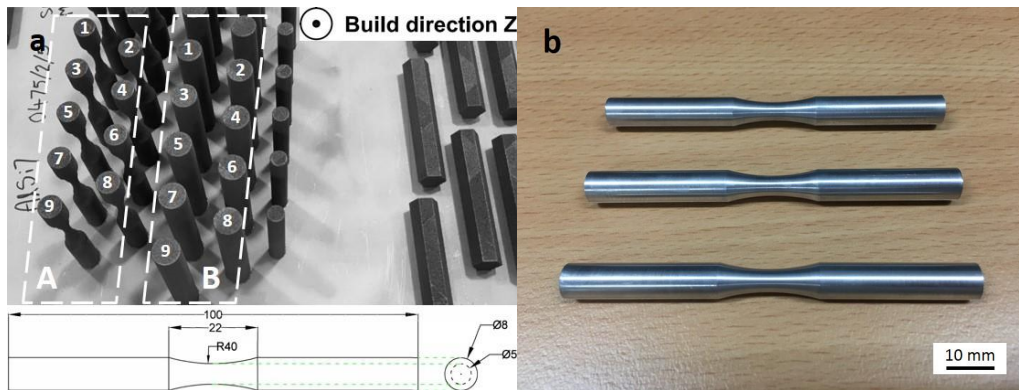


Figure 3. (a) Fatigue samples built by SLM at two directions; (b) Fatigue samples after machining based on the dimension illustrated in (a)

Following SLM process, all the fatigue sample bars were solution heat treated and artificially aged (Rao et al., 2017b). Samples from group B were then machined into fatigue specimens with the dimensions

illustrated (Figure 3a). It should be noted that after machining, the surface roughness ( $R_a$ ) for samples from group B was all below  $0.2 \mu\text{m}$  (Figure 3b). The fatigue tests were all performed at room temperature under axial tension according to ASTM standard E466-07 (Designation, 2007), using a frequency of 20 Hz, a stress ratio ( $R = \sigma_{\min}/\sigma_{\max}$ ) of 0.1 with three maximum stress levels of 100 MPa, 150 MPa, and 200 MPa applied. Three fatigue samples were tested at each stress level from each batch of specimens from group A and B with the run-out cycle of  $2.1 \times 10^6$ , and the surviving samples were identified as run outs.

After mechanical testing, the surface roughness morphology of the A357 fatigue samples was also observed by optical microscope (OM), and then measured by Mitutoyo Surftest SJ-410 series surface roughness tester. Three measurements were carried out at each condition to get average results. Fractographic features were determined using a FEI Quantas 3D field emission scanning electron microscopy (SEM) operating at 15 keV in the secondary electron imaging (SEI) mode.

## RESULTS AND DISCUSSION

### Surface Roughness for Net-shaped Samples

#### Microstructure Analysis

The defect distribution for the surfaces of the net-shaped samples was determined by OM (Figure 4). Irregular surface features, such as balling and satellites, are observed. In comparison to the net-shaped samples (Figure 4), the surface roughness of the as-machined samples ( $<0.2 \mu\text{m}$ ) is much better (Figure 3b).

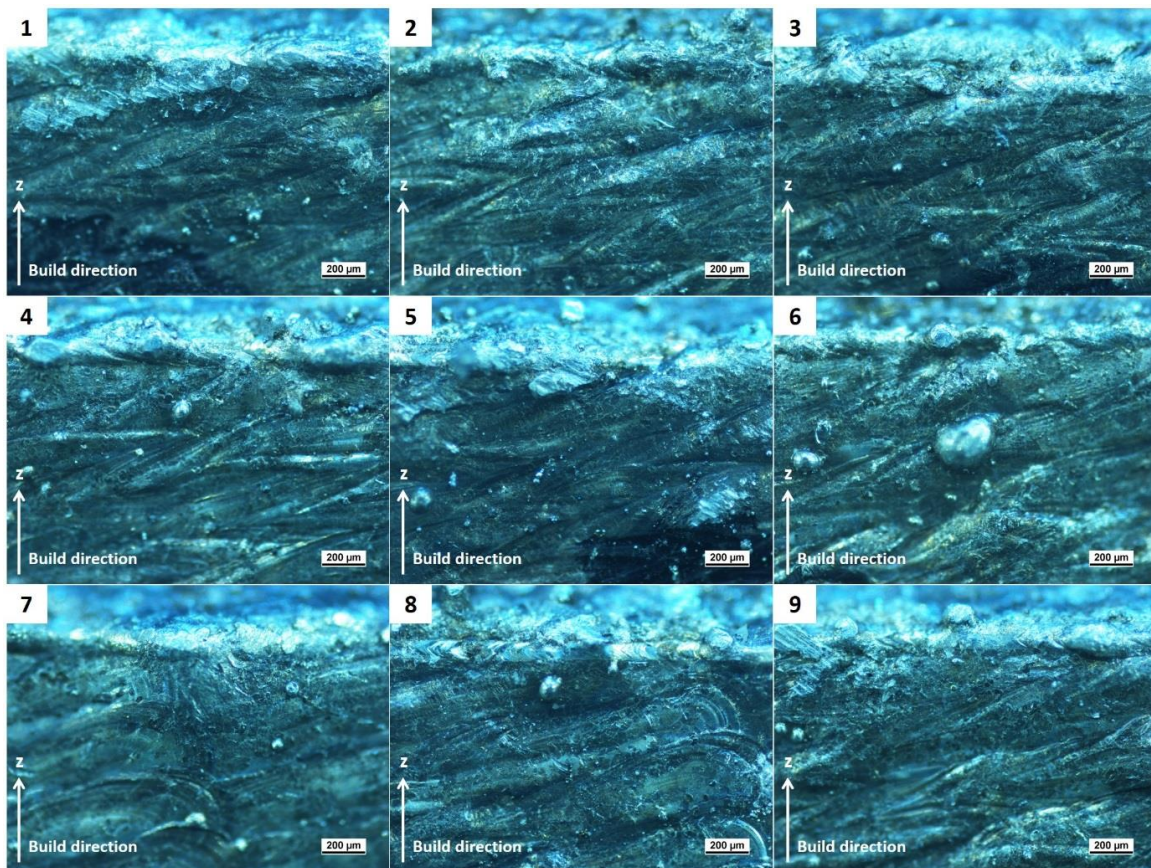


Figure 4. The surface roughness of the net-shaped fatigue (group A) samples in the as-built condition along the BD (z axis)

## Roughness Measurements

The surface morphology of the fatigue samples in their as-fabricated condition without post-processing machining are also measured (Figure 5). The Ra for each sample corresponds to Rz quite well. In general, for the net-shaped samples with a poor surface roughness, such as sample 6 with the existence of large particles, they possess much higher Rz value with larger standard deviation, indicating a larger range of unmelted particle size with poorer distribution. This is due to the less optimised laser parameters applied, generating porosities and defects (Rao et al., 2016). These defects could all potentially decrease the fatigue strength of SLMed parts (Aboulkhair et al., 2016).

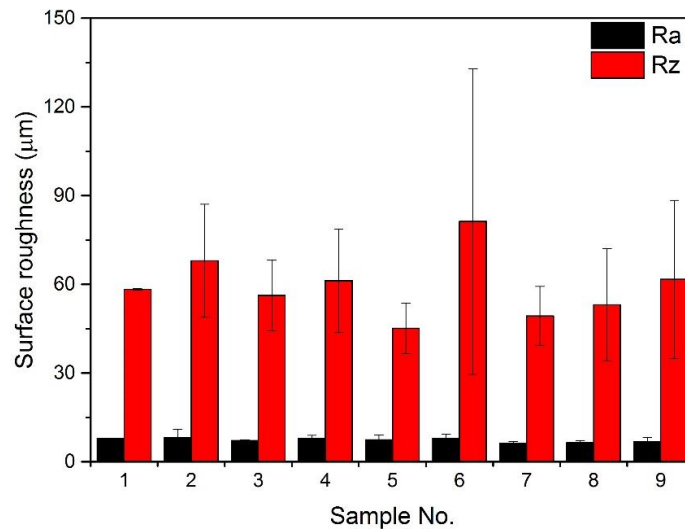


Figure 5. The surface roughness of the net-shaped fatigue (group A) samples in the as-built condition along the BD, where Ra refers to the arithmetic mean of the absolute values of the surface departures from the mean plane, and Rz the average of ten highest and lowest roughness points in the dataset

## **Fatigue Performance**

### Stress-Cycle (SN) Curves

The fatigue life of machined SLMed A357 is close to that of as-cast A357 alloy (Figure 6) (Serrano-Munoz et al., 2016; Tang & Pistorius, 2017). The S-N curves of the fatigue samples show that only two of the machined samples (group B) in this study, where the lowest maximum stress level examined was 100 MPa, exceeded the pre-defined run-out limit of  $2.1 \times 10^6$  cycles.

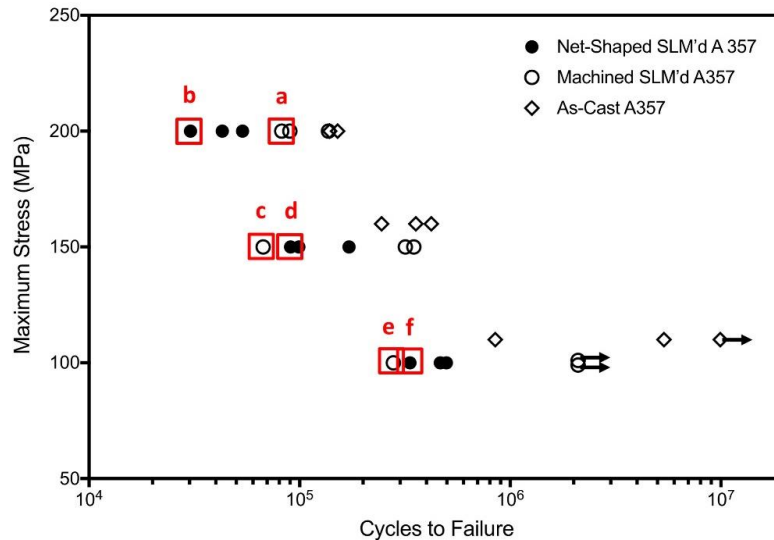


Figure 6. S-N curves for all the investigated conditions for both group A and B samples showing the effects of machining on the fatigue behaviours of SLMed A357 alloy. The fatigue performance for as-cast Al alloy A357 is also included for reference (Serrano-Munoz et al., 2016)

Also, it should be noted that the S-N data for samples with or without machining cannot be generalised over the range of stress levels. For instance, the difference between the fatigue life of the net-shaped and machined samples gets larger with the decrease of the maximum stress levels (Figure 6). At the maximum stress of 200 MPa, the fatigue life of the net-shaped samples is consistently lower than that of the machined sample. At the maximum stress level of 150 MPa, the fatigue life of the machined samples is still better than that of the net-shaped sample with one exception: the machined sample marked as “c” has the lowest fatigue life than all the other samples. Similarly, at the maximum stress level of 100 MPa, the fatigue life of two machined samples reached the pre-defined run-out limit, which is one order higher than that of all net-shaped samples. However, there is also one machined sample (marked as “e”) possessing much shorter fatigue life than the net-shaped samples.

This suggests that machining improves the fatigue life of SLMed samples particularly at lower stress levels. This is potentially because the fatigue life for the SLMed materials is initiation dominated at low stresses and propagation dominated at high stresses (Aboulkhair et al., 2016). In this regard, surface roughness has a greater effect on fatigue initiation at lower stress levels (Figure 6). For some of the machined samples still possessing quite low number of cycles before failure, this is because of the defects and large strain induced during post-machining, leading to a wider range of variability in the material's performance.

### Fractography

For further investigation on the fatigue crack initiation and propagation in both net-shaped and machined SLMed A357 specimens, failure analysis on the fatigue surfaces was also carried out (Figure 7). During fatigue testing with a stress level lower than the yield point, crack initiation process is commonly considered as dominating the fatigue life (Krupp, 2007; K. Zhang, Yang, Huang, Wu, & Davies, 2015). It is obvious that the crack initiation in the machined samples was associated to the presence of sub-surface defects such as porosity (Figure 7a) and large oxidised regions (Figure 7c and Figure 7e). The presence of the oxidised regions on the fracture surfaces of the machined samples “c” and “e” is suspected to attribute to the significantly lower fatigue life than the other machined samples tested at the same stress level (Figure 6). Also, it is quite likely that those relatively large (micron-sized or larger) oxidised regions potentially present in the fracture surfaces are formed by the oxidation of vaporised selective laser melted alloys (Tang & Pistorius, 2017). This still needs further work to confirm in the near future.

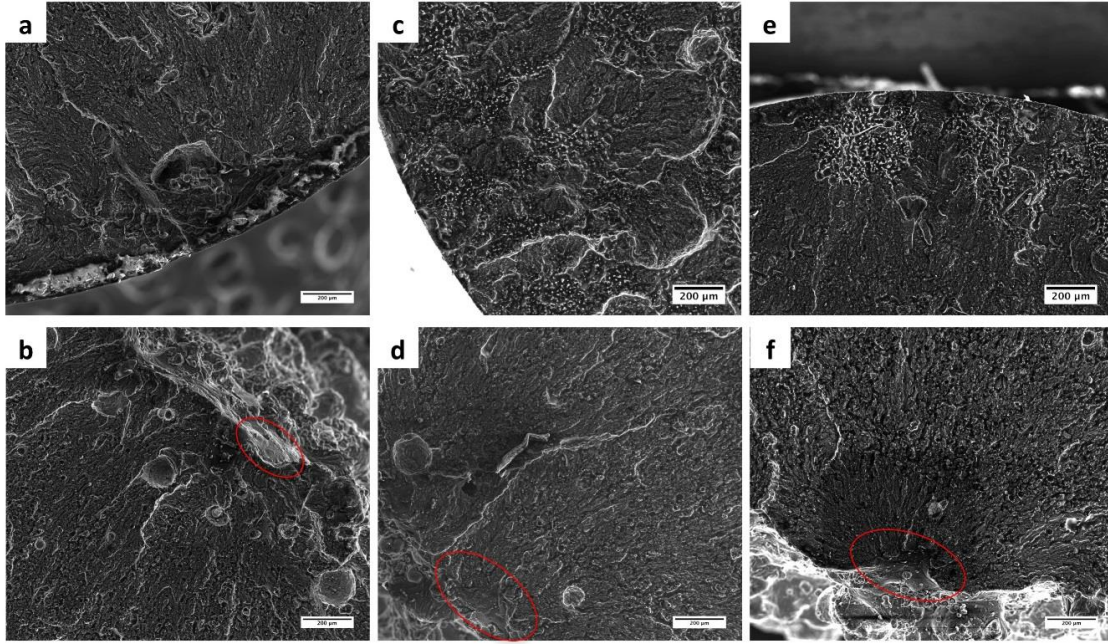


Figure 7. SEM micrographs showing crack initiation sites of fatigue samples from group A and B, corresponding to the number of cycle points labelled a, b, c, d, e, and f in Figure 6, where samples labeled as a, c, and e are machined ones and labeled as b, d, and f are net-shaped ones. The surface features that may cause the crack initiation in net-shaped samples are marked by the red ovals

In contrast, the crack initiation in the net-shaped samples is more related to the rougher selective laser melted surface instead of the sub-surface defects. For instance, the crack initiation in sample “f” starts from a penetrated wedge-shaped surface feature (marked by the red oval in Figure 7f). Similar surface features are present and marked on the fracture surfaces of sample “b” and “d”, which seem to trigger crack initiation on both samples. Those wedge-shaped surfaces could accumulate higher stresses on their tips or notches, and thus are detrimental to the fatigue resistance of the SLMed A357 samples (Frost, Marsh, & Pook, 1974; K Zhang, Yang, Lim, Wu, & Davies, 2017).

Therefore, it is evident that the fatigue life of SLMed net-shaped samples is shorter than those with machined surfaces (Aboulkhair et al., 2016; Tang & Pistorius, 2017). This has been attributed to the poor surface roughness commonly found in the net-shaped samples (Figure 4 and Figure 5), generating preferred sites for fatigue crack initiation.

## CONCLUSIONS

The fatigue resistance of selective laser melted A357 specimens printed in the Z direction under both net-shaped and machined conditions was studied. The morphology of surface roughness and fractography of the fatigue samples were all investigated to clarify the mechanisms for crack initiation. In the net-shaped SLMed fatigue samples, cracks were initiated because of the rough surfaces. Post-machining largely improves the surface finish of the SLMed samples, correspondingly enhancing the fatigue lives. In this regard, the fatigue life of machined SLMed A357 samples is comparable to that of the conventional cast alloys. In addition, the mechanism of fatigue crack initiation in machined SLMed A357 is dominated by the presence of defects. Failure under cyclic loading always originates at surface or sub-surface defects, this being the weaker region in the Al-rich matrix for SLMed A357 alloy.

## ACKNOWLEDGMENTS

This work was supported by Monash University (Australia), Science & Industry Endowment Fund (SIEF) under the program [RP04-153] “Manufacturing a small demonstrator aero-engine entirely through additive manufacturing”, and Australia Research Council [IH130100008] “Industrial Transformation Research Hub (ITRH) for Transforming Australia’s Manufacturing Industry through High Value Additive Manufacturing”, including financial support from Safran Power Units (France) and Amaero Engineering (Australia). The authors are also grateful for the access to the facilities at Monash Centre for Additive Manufacturing (MCAM) and Monash Centre for Electron Microscopy (MCEM).

## REFERENCES

- Aboulkhair, N. T., Maskery, I., Tuck, C., Ashcroft, I., & Everitt, N. M. (2016). Improving the fatigue behaviour of a selectively laser melted aluminium alloy: Influence of heat treatment and surface quality. *Materials & Design*, *104*, 174-182. <http://dx.doi.org/10.1016/j.matdes.2016.05.041>
- Brandl, E., Heckenberger, U., Holzinger, V., & Buchbinder, D. (2012). Additive manufactured AlSi10Mg samples using Selective Laser Melting (SLM): Microstructure, high cycle fatigue, and fracture behavior. *Materials & Design*, *34*(0), 159-169. <http://dx.doi.org/10.1016/j.matdes.2011.07.067>
- Designation, A. (2007). E466-07, Standard practice for conducting force controlled constant amplitude axial fatigue tests of metallic materials. *ASTM International*.
- Fox, J. C., Moylan, S. P., & Lane, B. M. (2016). Effect of Process Parameters on the Surface Roughness of Overhanging Structures in Laser Powder Bed Fusion Additive Manufacturing. *Procedia CIRP*, *45*(Supplement C), 131-134. <https://doi.org/10.1016/j.procir.2016.02.347>
- Frost, N. E., Marsh, K. J., & Pook, L. P. (1974). *Metal fatigue*: Courier Corporation.
- Krupp, U. (2007). *Fatigue crack propagation in metals and alloys: microstructural aspects and modelling concepts*: John Wiley & Sons.
- Martin, J. H., Yahata, B. D., Hundley, J. M., Mayer, J. A., Schaedler, T. A., & Pollock, T. M. (2017). 3D printing of high-strength aluminium alloys. *Nature*, *549*(7672), 365-369.
- Prashanth, K., Scudino, S., & Eckert, J. (2017). Defining the tensile properties of Al-12Si parts produced by selective laser melting. *Acta Materialia*, *126*, 25-35.
- Rao, H., Giet, S., Yang, K., Wu, X., & Davies, C. H. J. (2016). The influence of processing parameters on aluminium alloy A357 manufactured by Selective Laser Melting. *Materials & Design*, *109*, 334-346. <http://dx.doi.org/10.1016/j.matdes.2016.07.009>
- Rao, H., Wu, X., & Davies, C. (2017a). *Microstructure evolution and strengthening mechanisms of aluminium alloy A357 manufactured by Selective Laser Melting*. Paper presented at the 17th Australian International Aerospace Congress: AIAC 2017.
- Rao, J. H., Zhang, Y., Fang, X., Chen, Y., Wu, X., & Davies, C. H. J. (2017b). The origins for tensile properties of selective laser melted aluminium alloy A357. *Additive Manufacturing*, *17*, 113-122. <https://doi.org/10.1016/j.addma.2017.08.007>
- Serrano-Munoz, I., Buffiere, J. Y., Verdu, C., Gaillard, Y., Mu, P., & Nadot, Y. (2016). Influence of surface and internal casting defects on the fatigue behaviour of A357-T6 cast aluminium alloy. *International Journal of Fatigue*, *82*(Part 3), 361-370. <https://doi.org/10.1016/j.ijfatigue.2015.07.032>

- Siddique, S., Imran, M., & Walther, F. (2017). Very high cycle fatigue and fatigue crack propagation behavior of selective laser melted AlSi12 alloy. *International Journal of Fatigue*, *94*, 246-254.
- Tang, M., & Pistorius, P. C. (2017). Oxides, porosity and fatigue performance of AlSi10Mg parts produced by selective laser melting. *International Journal of Fatigue*, *94*, 192-201.
- Uzan, N. E., Shneck, R., Yeheskel, O., & Frage, N. (2017). Fatigue of AlSi10Mg specimens fabricated by additive manufacturing selective laser melting (AM-SLM). *Materials Science and Engineering: A*, *704*, 229-237. <https://doi.org/10.1016/j.msea.2017.08.027>
- Wang, P., Sin, W., Nai, M., & Wei, J. (2017). Effects of Processing Parameters on Surface Roughness of Additive Manufactured Ti-6Al-4V via Electron Beam Melting. *Materials*, *10*(10), 1121.
- Zhang, K., Yang, K., Lim, S., Wu, X., & Davies, C. (2017). Effect of the presence of macrozones on short crack propagation in forged two-phase titanium alloys. *International Journal of Fatigue*, *104*, 1-11.
- Zhang, K., Yang, K. V., Huang, A., Wu, X., & Davies, C. H. J. (2015). Fatigue crack initiation in as forged Ti-6Al-4V bars with macrozones present. *International Journal of Fatigue*, *80*(Supplement C), 288-297. <https://doi.org/10.1016/j.ijfatigue.2015.05.020>